ISSN 0022-4766, Journal of Structural Chemistry, 2019, Vol. 60, No. 8, pp. 1314-1326. © Pleiades Publishing, Inc., 2019.
Russian Text © The Author(s), 2019, published in Zhurnal Strukturnoi Khimii, 2019, Vol. 60, No. 8, pp. 1366-1378.

SYNTHESIS, STRUCTURE, MAGNETIC AND PHOTOLUMINESCENT PROPERTIES OF LANTHANIDE(III) COMPLEXES WITH A LIGAND BASED ON 1,10-PHENANTHROLINE AND (+)–3-CARENE

Yu. A. Bryleva[1,4]*, L. A. Glinskaya[1], A. M. Agafontsev[2,4], M. I. Rakhmanova[1], A. S. Bogomyakov[3,4], T. S. Sukhikh[1,4], E. A. Gorbunova[1,4], A. V. Tkachev[2,4], and S. V. Larionov[1,4]†

Ionic complexes of the composition $[LnL_2(NO_3)_2]_2[Ln(NO_3)_5]3Me_2CO$ (Ln = Sm (**1**), Eu (**2**), Tb (**3**), Dy (**4**)) with an optically active ligand **L** containing 1,10-phenanthroline and (+)–3-carene moieties are synthesized. According to the X-ray crystallographic data, the crystal structure of compound **2** is composed of complex $[EuL_2(NO_3)_2]^+$ cations (N_6O_4 polyhedron) and complex $[Eu(NO_3)_5]^{2-}$ anions (O_{10} polyhedron), and also Me_2CO molecules. The **L** and NO_3 ligands perform both tridentate and bidentate chelating functions respectively. Complexes **1**-**4** are isostructural and crystallize in the non-centrosymmetric space group *P*1; their magnetic properties are studied in the temperature range 2-300 K. The μ_{eff} values for **1**-**4** at 300 K are 3.14 μ_B, 6.08 μ_B, 16.76 μ_B, and 18.30 μ_B respectively and are typical of Ln^{3+} ions. For complex **3** significant anisotropy results in a nonlinear field dependence of the magnetization at 2 K. Complexes **1**-**4** exhibit metal-centered orange (Sm^{3+}), red (Eu^{3+}), green (Tb^{3+}), and yellow (Dy^{3+}) luminescence in the solid state at room temperature. Luminescence quantum yield decreases for solid samples in the order **2** > **1** > **3** ≈ **4**.

DOI: 10.1134/S0022476619080110

Keywords: lanthanides, complexes, terpenes, (+)–3-carene, structure, magnetic properties, photoluminescence.

INTRODUCTION

In coordination chemistry and chemistry of materials much attention is paid to the preparation of luminescent complexes of lanthanides (Ln) with diverse types of organic ligands [1-9]. Many of these complexes are stable in the air atmosphere in both solid phase and solutions. It is important that Ln^{3+} complexes can exhibit narrow intense emission bands

[1]Nikolaev Institute of Inorganic Chemistry, Siberian Branch, Russian Academy of Sciences, Novosibirsk, Russia; *bryleva@niic.nsc.ru. [2]Vorozhtsov Institute of Organic Chemistry, Siberian Branch, Russian Academy of Sciences, Novosibirsk, Russia. [3]International Tomography Center, Siberian Branch, Russian Academy of Sciences, Novosibirsk, Russia. [4]Novosibirsk State University, Novosibirsk, Russia. Original article submitted February 21, 2019; revised February 28, 2019; accepted February 28, 2019.

in the visible and near-IR spectral ranges, which provides the possibility of using Ln complexes to obtain luminescent devices and biosensors. One of the best antenna ligands is 1,10-phenanthroline (phen) [10]. In particular, $[Ln(phen)_2(NO_3)_3]$ complexes were obtained and studied [11-20]. The $[Eu(phen)_2(NO_3)_3]$ complex exhibits red photoluminescence (PL) in the solid state [14, 16, 18, 20]. The luminescence quantum yield of this compound dissolved in CH_3CN is 21% [16]. It is found that the use of methyl derivatives instead of archetypal phen as a ligand caused an increase in the quantum yield to 27% [16]. It is promising to obtain and study the structure and luminescent properties of Ln^{3+} complexes with phen derivatives having much larger substituents than the methyl group. The application of chiral phen derivatives as ligands is of special interest. At present, the synthesis of Ln(III) complexes with various chiral ligands attracts much attention [21, 22]. It is due to that these complexes exhibit circular dichroism and circularly polarized luminescence, can serve as materials for nonlinear optics and also as ferroelectric materials and chiral molecular magnets. Low-toxic natural terpene derivatives with a high enantiomeric purity take an important place among chiral ligands. Ln complexes with terpyridine [23] and 2,2′-bipyridine [24] derivatives have been described. We have previously obtained and studied $[LnL'_2(NO_3)_3]$ (Ln = Eu, Gd, Tb, Dy) compounds with a ligand containing 1,10-phenanthroline and (–)-menthol fragments [25]. It is found that the Eu^{3+} complex with this ligand has a high quantum yield (φ = 87%).

The aim of this work was the synthesis and analysis of the structure, magnetic and photoluminescent properties of Ln(III) (Ln = Sm, Eu, Tb, Dy) complexes with a new optically active 2-((3bS,4aR)-3,4,4-trimethyl-3b,4,4a,5-tetrahydro-2H-cyclopropa[3,4]cyclopenta[1,2-c]pyrazol-2-yl)-1,10-phenanthroline ligand (**L**) containing a fragment of natural terpene – (+)–3-carene (Scheme 1).

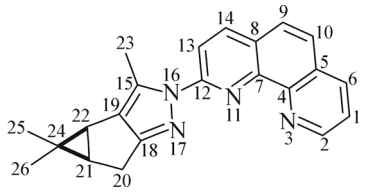

Scheme 1. Structure of ligand **L**. Atom numbering is given for the description of NMR spectra.

EXPERIMENTAL

For the synthesis of $Tb(NO_3)_3·6H_2O$ compounds, CuI, K_2CO_3, DMF, $NH_{3(aq)}$, sodium tartrate, $CHCl_3$, Na_2SO_4, CH_2Cl_2, EtOAc (reagent grade), $Eu(NO_3)_3·6H_2O$, $Sm(NO_3)_3·6H_2O$, $Dy(NO_3)_3·6H_2O$ (high purity grade), and Me_2CO (special purity grade) were used. 2-Chlorophenanthroline was synthesized from 1,10-phenanthroline by the procedure described in [26]. (3bS,4aR)-3,4,4-Trimethyl-3b,4,4a,5-tetrahydro-2H-cyclopropa[3,4]cyclopenta[1,2-c]pyrazole was prepared by the known procedure [27, 28].

Synthesis of 2-((3bS,4aR)-3,4,4-trimethyl-3b,4,4a,5-tetrahydro-2H-cyclopropa[3,4]cyclopenta[1,2-c]pyrazol-2-yl)-1,10-phenanthroline (L). Into a round-bottom flask containing 2.14 g (10 mmol) of 2-chlorophenanthroline, 1.62 g (10 mmol) of (3bS,4aR)-3,4,4-trimethyl-3b,4,4a,5-tetrahydro-2H-cyclopropa[3,4]cyclopenta[1,2-c]pyrazole, 0.50 g (2.6 mmol) of CuI, and 2.76 g (20 mmol) of K_2CO_3, 20 mL of DMF were added and heated to 90-95 °C with stirring in an argon flow until the spot of the initial compound disappeared in thin layer chromatography (TLC) (24 h). After the completion of the reaction, the reaction mixture was poured into a solution containing 100 mL of water, 30 mL of aqueous ammonia, and 10 g of sodium tartrate, and then extracted with chloroform (3×100 mL). The combined organic phases were dried with Na_2SO_4, filtered from the dryer, and the solvent was removed under reduced pressure. The product was isolated by column chromatography on silica gel (eluent – CH_2Cl_2:EtOAc = 2:1). Yield 2.21 g (65%). T_{melt} 175 °C (from EtOAc), $[\alpha]_{589}^{28.6}$ - 150 (s, 0.316, $CHCl_3$). IR spectrum (ν, cm^{-1}): C–H 3030, 2970–2840. High-resolution mass spectrum, found: *m*/*z*

340.1681 [M^+], $C_{22}H_{20}N_4$. Calculated: M = 340.1683. Mass spectrum (EI, 70 eV), m/z (I_{rel}(%)): 340 (48), 325 (100), 179 (19), 118 (63), 116 (66).

^{1}H NMR ($CDCl_3$ δ, ppm): 0.75 (s, 3H, H(26)), 1.12 (s, 3H, H(25)), 1.75 (dd, J = 7.0, J = 6.5, 1H, H(22)), 1.86 (d, J = 7.0, 1H, H(21)), 2.60 (d, J = 16.6, 1H, H(20α)), 2.87 (dd, J = 16.6, J = 6.5, 1H, H(20β)), 3.00 (s, 3H, H(23)), 7.51 (dd, J = 7.8, J = 4.2, 1H, H(1)), 7.60 (d, J = 8.5, 1H, H(10)), 7.66 (d, J = 8.5, 1H, H(9)), 8.12 (dd, J = 7.8, J = 1.6, 1H, H(6)), 8.17 (m, 2H, H(13 and 14)), 9.08 (dd, J = 4.2, J = 1.6, 1H, H(2)). ^{13}C NMR ($CDCl_3$, δ, ppm): 14.49 (C(23)), 14.60 (C(26)), 23.20 (C(24)), 24.45 (C(20)), 26.12 (C(21)), 26.88 (C(25)), 34.18 (C(22)), 116.18 (C(13)), 122.36 (C(1)), 124.75 (C(10)), 125.80 (C(19)), 125.99 (C(9)), 128.80 (C(15)), 135.38 (C(6)), 135.46 (C(8)), 137.49 (C(14)), 137.73 (C(5)), 144.45 (C(4)), 146.16 (C(7)), 149.84 (C(2)), 153.22 (C(12)), 164.49 (C(18)).

Synthesis of $[SmL_2(NO_3)_2]_2[Sm(NO_3)_5]\cdot 3Me_2CO$ (1). To a solution of 0.044 g (0.10 mmol) of Sm(NO3)3·6H_2O in 1 mL of acetone, a solution of 0.045 g (0.13 mmol) of the ligand **L** in 4 mL of acetone was added with stirring. A white precipitate formed after stirring the solution for 3.5 h. The product was filtered off, washed with acetone, and dried in a desiccator over anhydrone at room temperature. Yield 0.048 g (55%). Found, %: C 45.0, H 3.8, N 13.8. Calculated for $C_{97}H_{98}N_{25}O_{30}Sm_3$, %: C 45.8, H 3.9, N 13.8. IR spectrum (ν, cm^{-1}): 2952 w, 2923 w, 1712 m, 1626 w, 1609 m, 1590 m, 1572 m, 1519 s, 1502 s, 1480 s, 1452 s, 1423 s, 1403 m, 1365 s, 1339 m, 1303 m, 1221 w, 1152 w, 1122 m, 1074 m, 1028 m, 927 w, 871 w, 855 m, 816 w, 788 m, 740 m, 726 w, 649 w, 583 w, 529 w, 428 w.

Synthesis of $[LnL_2(NO_3)_2]_2[Ln(NO_3)_5]\cdot 3Me_2CO$ (Ln = Eu (2), Tb (3), Dy (4)) was performed by the above described procedure. Yields 45%, 65%, and 65% respectively.

For **2** found, %: C 45.1, H 3.8, N 13.9. Calculated for $C_{97}H_{98}N_{25}O_{30}Eu_3$,%: C 45.7, H 3.9, N 13.7. IR spectrum (ν, cm^{-1}): 2953 w, 2924 w, 1712 m, 1626 w, 1608 m, 1589 m, 1572 m, 1519 s, 1503 s, 1480 s, 1453 s, 1423 s, 1402 m, 1365 s, 1337 m, 1304 s, 1220 w, 1152 w, 1123 m, 1074 m, 1027 m, 927 w, 870 w, 854 m, 816 w, 788 m, 740 m, 726 w, 647 w, 582 w, 529 w, 427 w.

For **3** found, %: C 45.4, H 3.8, N 14.0. Calculated for $C_{97}H_{98}N_{25}O_{30}Tb_3$, %: C 45.3, H 3.8, N 13.6. IR spectrum (ν, cm^{-1}): 2956 w, 2925 w, 1712 m, 1627 w, 1609 m, 1591 m, 1573 m, 1519 s, 1503 s, 1482 s, 1453 s, 1423 s, 1403 m, 1367 s, 1338 m, 1308 s, 1221 w, 1151 w, 1123 m, 1075 m, 1029 m, 926 w, 871 w, 855 m, 815 w, 788 m, 742 m, 727 w, 649 w, 582 w, 530 w, 428 w.

For **4** found, %: C 44.8, H 3.8, N 13.9. Calculated for $C_{97}H_{98}N_{25}O_{30}Dy_3$, %: C 45.1, H 3.8, N 13.6. IR spectrum (ν, cm^{-1}): 2954 w, 2923 w, 1712 m, 1627 w, 1609 m, 1590 m, 1573 m, 1519 s, 1503 s, 1481 s, 1453 s, 1423 s, 1404 m, 1366 s, 1339 m, 1308 s, 1221 w, 1153 w, 1123 m, 1076 m, 1029 m, 927 w, 870 w, 854 m, 814 w, 789 m, 743 m, 728 w, 648 w, 583 w, 529 w, 428 w.

The C, H, N elemental analysis was carried out on a Euro EA 3000 analyzer. The IR spectra of compounds **1**-**4** were measured in KBr pellets in the range 4000-400 cm^{-1} on a Scimitar FTS2000 spectrophotometer. The IR spectrum of **L** in KBr was recorded on a Brucker TENSOR 27 instrument. For TLC the PTLC-AF-A-UV Sorbfil plates with a fixed sorbent (SiO_2) layer and a UV indicator were used. To visualize the components of mixtures under study the plates were irradiated with a UV lamp and kept in iodine vapor. For column chromatography silica gel with a grain size of 0.050-0.160 mm (Imid) was used. The melting point of the **L** compound was determined by differential scanning calorimetry on a NETZSCH STA 409 instrument. Optical rotation values were measured on a PolAAr 3005 polarimeter; concentrations are given in g/100 mL. The mass spectrum of **L** was measured on a Bruker micrOTOF-Q spectrometer. NMR spectra of **L** were recorded on a Bruker DRX-500 spectrometer (^{1}H – 500.13 MHz, ^{13}C – 125.77 MHz) for a solution with a concentration of 5-10 mg/mL at 30 °C. Solvent ($CDCl_3$) signals were used as the internal standard: δH = 7.24 ppm, δC = 76.90 ppm. Thermal decomposition was investigated on a NETZSCH TG 209 F1 thermoanalyzer in the temperature range 20-600 °C in the helium atmosphere (gas flow rate 30 mL/min, heating rate 10 deg/min, sample weight 5-6 mg). Powder X-ray diffraction (XRD) of the complexes was performed on a Shimadzu XRD-7000 diffractometer (CuK_α radiation, Ni filter, Bragg–Brentano geometry). Samples for powder XRD were prepared as follows: the polycrystals were ground in an agate mortar in the presence of

heptane. The suspension obtained was deposited on a polished side of the standard quartz cuvette. After evaporation of heptane, the sample represented a uniform thin layer (~100 μm thick).

For a single crystal of compound **2**, the position and unit cell parameters and reflection intensities were measured at 150 K on an automated Bruker X8 APEX CCD diffractometer equipped with a two-dimensional detector by the standard procedure (MoK_α radiation, λ = 0.71073 Å, graphite monochromator). Crystallographic characteristics, details of the XRD experiment and structure refinement of **2** are summarized in Table 1. The structure was solved by a direct method and refined by the full-matrix least-squares technique in the anisotropic approximation for non-hydrogen atoms using the SHELXL-2014 program package [29]. Positions of all H atoms were found from difference Fourier maps and included in the refinement with the riding model. Main interatomic distances and bond angles are listed in Table 2. Single crystal XRD data for complex **2** have been deposited with the Cambridge Crystallography Data Center under number 1896703 and can be received from the authors or at http://www.ccdc.cam.ac.uk/conts/retrieving.html.

The magnetic susceptibility χ of solid samples of complexes **1**-**4** was measured on a SQUID- MPMS XL (Quantum Design) magnetometer in the temperature range 2-300 K at a magnetic field strength of 5 kOe. Paramagnetic components of the magnetic susceptibility were determined with taking into account a diamagnetic contribution estimated from Pascal constants. The effective magnetic moment μ_{eff} was calculated by the formula $\mu_{eff} = [3k\chi T/(N_A\mu_B^2)]^{1/2}$, where N_A, μ_B, and k are the Avogadro number, the Bohr magneton, and the Boltzmann constant respectively.

The luminescence excitation and emission spectra of complexes **1**-**4** and the **L** ligand as well as PL lifetimes were measured at 300 K on a Fluorolog-3 (Horiba Jobin Yvon) spectrofluorimeter with a cooled PC177CE-010 photon detection module equipped with FEU R2658. The instrument is equipped with a system measuring PL lifetimes based on time-correlated counting of single photons to measure emission quenching kinetics. To measure lifetimes in the nanosecond range the instrument was equipped with a set of solid state lasers with different wavelengths. To measure the absolute quantum yield of solid samples a Quanta-φ integral sphere was used.

TABLE 1. Crystallographic Characteristics, Details of the Experiment and Structure Refinement of Compound **2**

Empirical formula	$C_{97}H_{98}Eu_3N_{25}O_{30}$
Molecular weight	2549.88
Crystal system	Triclinic
Space group	*P*1
a, *b*, *c*, Å	13.155(1), 14.828(1), 16.336(2)
α, β, γ, deg	63.086(2), 75.528(4), 65.350(2)
V, Å^3	2575.0(4)
Z; ρ_{calc}, mg/cm^3	1, 1.644
μ, mm^{-1}	1.897
Crystal dimensions, mm	0.2×0.17×0.13
2θ scanning range, deg	3.292-54.404
Number of meas. /indep. reflections	42833 / 21860
R(int)	0.0244
Number of reflections with $I > 2\sigma(I)$	21860
Number of refined parameters	1374
GOOF on F^2	1.021
R_1 / wR_2 ($I > 2\sigma(I)$)	0.0283 / 0.0675
R_1 / wR_2 (over all I_{hkl})	0.0307 / 0.0686
Residual electron density (max / min), e/Å^3	0.87 / –1.01
Flack parameter	–0.005(1)

TABLE 2. Selected Bond Lengths *d* and Bond Angles ω in the Structure of Compound **2**

Bond	*d*, Å	Bond	*d*, Å	Bond	*d*, Å
CATION 1		CATION 2		ANION	
Eu(1)–(1A)	2.585(5)	Eu(2)–N(1C)	2.596(5)	Eu(3)–O(13)	2.511(5)
Eu(1)–N(2A)	2.567(5)	Eu(2)–N(2C)	2.553(5)	Eu(3)–O(14)	2.464(5)
Eu(1)–(3A)	2.513(5)	Eu(2)–N(3C)	2.537(5)	Eu(3)–O(16)	2.458(5)
Eu(1)–(1B)	2.571(5)	Eu(2)–N(1D)	2.601(5)	Eu(3)–O(17)	2.477(5)
Eu(1)–(2B)	2.564(5)	Eu(2)–N(2D)	2.553(5)	Eu(3)–O(19)	2.494(5)
Eu(1)–N(3B)	2.524(5)	Eu(2)–N(3D)	2.541(5)	Eu(3)–O(20)	2.463(5)
Eu(1)–O(1)	2.560(5)	Eu(2)–O(7)	2.543(4)	Eu(3)–O(22)	2.554(5)
Eu(1)–O(2)	2.510(4)	Eu(2)–O(8)	2.517(4)	Eu(3)–O(23)	2.472(5)
Eu(1)–O(4)	2.521(4)	Eu(2)–O(10)	2.536(4)	Eu(3)–O(25)	2.515(5)
Eu(1)–O(5)	2.519(4)	Eu(2)–O(11)	2.502(4)	Eu(3)–O(26)	2.512(5)
Angle	ω, deg	Angle	ω, deg	Angle	ω, deg
O(1)–Eu(1)–N(1A)	111.1(2)	O(1)–Eu(2)–N(1C)	108.3(2)	O(13)–Eu(3)–O(16)	68.0(2)
O(1)–Eu(1)–N(2A)	70.5(2)	O(1)–Eu(2)–N(2C)	133.1(2)	O(13)–Eu(3)–O(17)	113.8(2)
O(1)–Eu(1)–N(3A)	129.9(2)	O(1)–Eu(2)–N(3C)	71.4(2)	O(13)–Eu(3)–O(19)	71.3(2)
O(1)–Eu(1)–(1B)	69.2(2)	O(1)–Eu(2)–N(1D)	68.3(2)	O(13)–Eu(3)–O(20)	114.5(2)
O(1)–Eu(1)–N(2B)	68.9(2)	O(1)–Eu(2)–N(2D)	92.4(2)	O(13)–Eu(3)–O(22)	167.7(2)
O(1)–Eu(1)–N(3B)	91.7(2)	O(1)–Eu(2)–N(3D)	72.1(2)	O(13)–Eu(3)–O(23)	117.0(2)
O(1)–Eu(1)–O(4)	136.2(1)	O(1)–Eu(2)–O(4)	140.1(1)	O(13)–Eu(3)–O(25)	71.5(2)
O(1)–Eu(1)–O(5)	158.8(1)	O(1)–Eu(2)–(5)	154.8(1)	O(13)–Eu(3)–O(26)	112.5(2)

RESULTS AND DISCUSSION

The ligand **L** was synthesized by a reaction of 2-chlorophenanthroline and (3bS,4aR)-3,4,4-trimethyl-3b,4,4a, 5-tetrahydro-2H-cyclopropa[3,4]cyclopenta[1,2-c]pyrazole in DMF in the presence of potassium carbonate as a base and copper(I) iodide as a catalyst (Scheme 2). Despite the possibility of arylation of the pyrazole derivative through both N atoms, only the **L** compound was obtained as a reaction product.

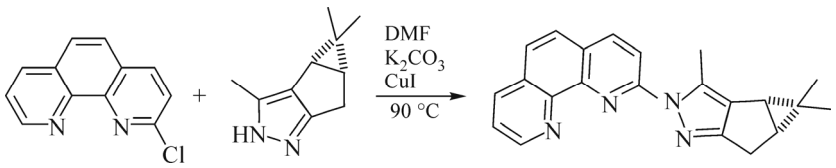

Scheme 2. Synthesis of the **L** ligand.

Coordination compounds **1**-**4** form as a result of the reaction of Ln(III) nitrates with the ligand **L** in acetone at a 3:4 mole ratio respectively

$$3Ln(NO_3)_3{\cdot}6H_2O + 4L \xrightarrow{\text{Acetone}} [LnL_2(NO_3)_2]_2[Ln(NO_3)_5]{\cdot}3Me_2CO\downarrow + 18H_2O.$$

The use of a larger amount of the ligand (Ln^{3+}:**L** = 1:3) results in the isolation of complexes of the same composition.

The analysis of the thermal properties of compounds **1**-**4** in the inert atmosphere in the temperature range 20-600 °C shows that steps clearly corresponding to the loss of three Me_2CO molecules are absent in TG curves. Fig. 1 depicts TG, DTA, and DTG curves of compound **1**; for compounds **2**-**4** similar curves are observed. On heating complexes **1**-**4** gradual

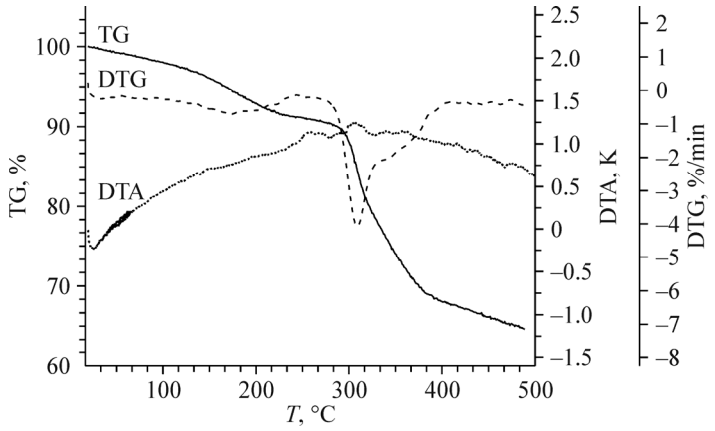

Fig. 1. TG, DTG, and DTA curves of compound **1**.

weight loss starts at 30 °C and continues up to ~240 °C. When this step is completed, the weight loss is ~10% and significantly exceeds the calculated acetone fraction in **1**-**4**, which is 6.8%, 6.8%, 6.8%, and 6.7% respectively. This step seems to correspond to the loss of solvate acetone molecules and partial decomposition of the complexes. At ~270 °C further decomposition starts. The weight loss is finished at T ~ 500 °C. The storage of compounds **1**-**4** at room temperature for several weeks does not lead to the removal of solvate acetone molecules, which indicates a sufficiently strong retention of Me_2CO molecules in the crystal lattice of the compounds.

The crystal structure of compound **2** has the ionic character. It is composed of two crystallographically independent $[EuL_2(NO_3)_2]^+$ complex cations, one $[Eu(NO_3)_5]^{2-}$ complex anion, and three solvate Me_2CO molecules. The structures of two independent cations and the complex anion are shown in Fig. 2. The cations are two spatial isomers (diastereoisomers) with different signs of the helicity of double π systems (Scheme 3). Both isomers have approximately a C_2 point group symmetry with a rotation axis passing through O3–Eu1–O6 and O9–Eu2–O12 atoms. These isomers form during the coordination to the Eu atom and cannot turn into each other without destructing the coordination bonds.

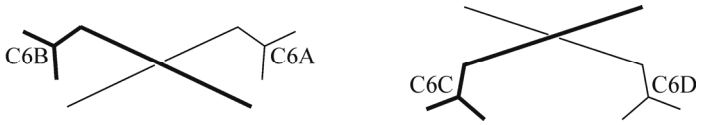

Scheme 3. Schematic representation of spatial isomers of $[EuL_2(NO_3)_2]^+$ cations.

In the cations the Eu atom coordinates six N atoms of two tridentate chelate **L** ligands with the Eu–N distances within 2.513(5)-2.601(5) Å and four O atoms of two bidentate chelate NO_3 ligands with Eu–O distances in the range 2.502(4)-2.560(5) Å (Table 2). This leads to the closing of two five-membered chelating rings EuN_2C_2 and two four-membered chelate rings EuO_2N. The coordination polyhedron N_6O_4 of the Eu atom (CN 10) has ten vertices. Both chelate EuN_2C_2 rings have the *envelope* conformation: the Eu(1) atom deviates from the N_2C_2 planes by 0.145(9) Å, –0.163(9) Å, 0.107(9) Å, and –0.182(9) Å (in cation 1); the Eu(2) atom deviates from the N_2C_2 planes by 0.078(9) Å, 0.260(8) Å, –0.048(9) Å, and –0.246(9)°Å (in cation 2). Angles between the planes of two EuN_2C_2 metallocycles are turned relative to each other at angles of 6.4(1)° and 6.2(4)° (in cation 1) and 3.6(1)° and 4.0(4)° (in cation 2). Dihedral angles between the planes of NO_3 groups and the central Eu(1) atom are 54.5(1)°; for Eu(2) this angle is 59.2(1)°.

In the $[Eu(NO_3)_5]^{2-}$ anion, the Eu atom coordinates ten O atoms of five bidentate chelate NO_3 ligands with Eu(1)–O distances within 2.463(5)-2.554(5) Å (Table 2). The coordination polyhedron of the Eu atom has ten vertices. Five EuO_2N chelating rings in the anion are almost planar: the average deviation from the mean planes does not exceed 0.006(3) Å. It should be noted that similar Ln(III) ionic complexes with 1,10-phen and 2,2′-bipyridine derivatives containing the

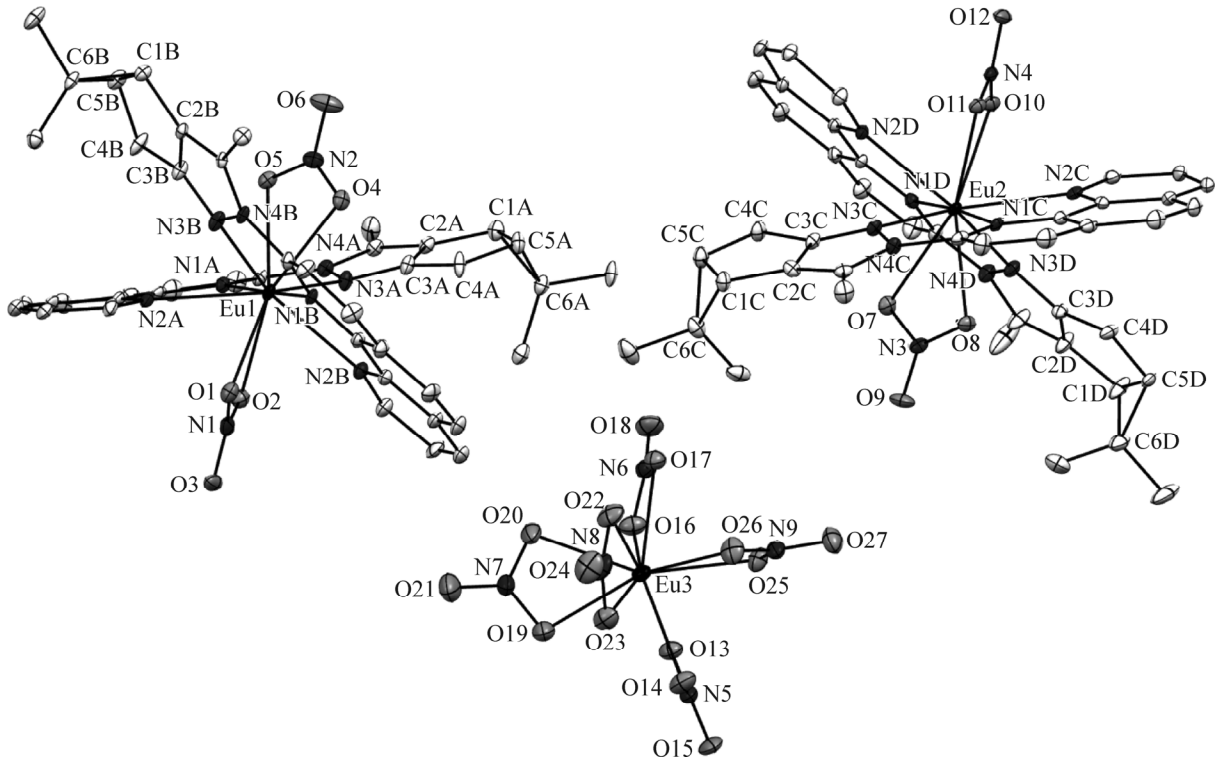

Fig. 2. Structure of two independent complex cations and the complex anion in the structure of compound **2**. H atoms are omitted. Thermal ellipsoids are shown at the 30% probability level.

$[Ln(NO_3)_5]^{2-}$ anion have been described in the literature. In particular, $[Eu(BTPhen)_2(NO_3)][Eu(NO_3)_5]$ (BTPhen = derivative of 2,9-bis(1,2,4-triazin-3-yl)-1,10-phenanthroline) [30] and $[Eu(CyMe_4\text{-}BTBP)_2(NO_3)][Eu(NO_3)_5]$ (BTBP = derivative of 6,6′-bis(1,2,4-triaxin-3-yl)-2,2′-bipyridine) [31] compounds in which nitrate groups are also coordinated in the bidentate chelate mode were synthesized and structurally characterized.

The pyrazole moiety condensed with a five-membered carbocycle (the average atomic deviation does not exceed 0.068(4) Å for cations 1 and 2), makes an angle of 19.5(1)° with the adjacent fragments of 14 atoms *via* common N(3)–N(4) edges. Dimethylcyclopropane fragments share C(1)–C(5) edges with the five-membered carbocycles and make dihedral angles with the planes of the five-membered rings of 112.8(3)°, 113.8(3)° (for cation 1) and 113.3°, 114.5(2)° (for cation 2).

The packing of ions and solvate acetone molecules is shown in (001) and (010) projections (Fig. 3). The cation packing makes channel cavities in which the anions and solvate acetone molecules are located (Fig. 3). The complex anions and acetone molecules alternate in these channels. In the absence of acetone molecules the cavity volume is 417 $Å^3$, and in the absence of anions and acetone molecules the total cavity volume is 806 $Å^3$ per cell. The channel radius is about 7.5 Å. The closest distance between Eu(1)…Eu(2) is 9.844 Å in the two cations and that between Eu(1)…Eu(3) and Eu(2)…Eu(3) is 8.209 Å and 8.415 Å in the cations and the anions respectively. A large distance between the ions facilitated the formation of the solvate.

Experimental and theoretical diffraction patterns of complex **2** are similar (Fig. 4). Diffraction patterns of the solid phases of compounds **1**-**4** are also similar to the theoretical diffraction pattern calculated based on the XRD data for the single crystal of **2**. Thus, all the samples studied are single-phase and isostructural to complex **2**.

IR spectra of complexes **1**-**4** exhibit absorption bands corresponding to antisymmetric stretching vibrations ν_3 of NO_3 groups at ~1480 cm^{-1}, ~1305 cm^{-1} and symmetric stretching vibrations ν_1 of these groups at ~1030 cm^{-1}. An appreciable splitting ν_3 (Δ = ~175 cm^{-1}) and the absence of a band at ~1390 cm^{-1} of the non-coordinated nitrate group indicate the bidentate chelate coordination of NO_3, which is consistent with the X-ray crystallographic data for complex **2** [32, 33]. Bands

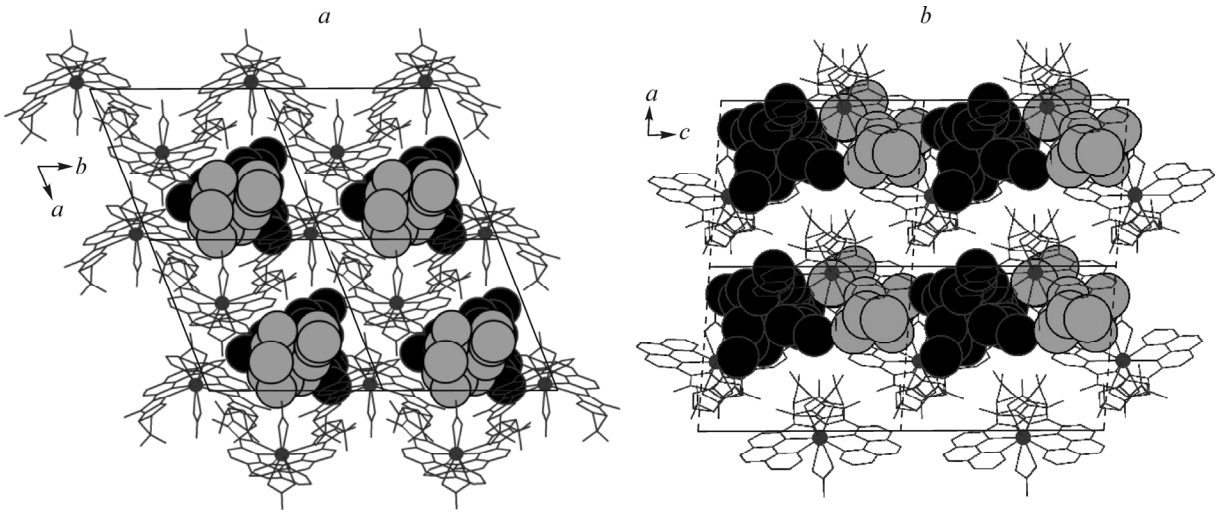

Fig. 3. Ion packing in the structure of **2** in the (001) (*a*) and (010) (*b*) projections. Anions are shown by dark Van der Waals spheres; acetone molecules are shown by light spheres.

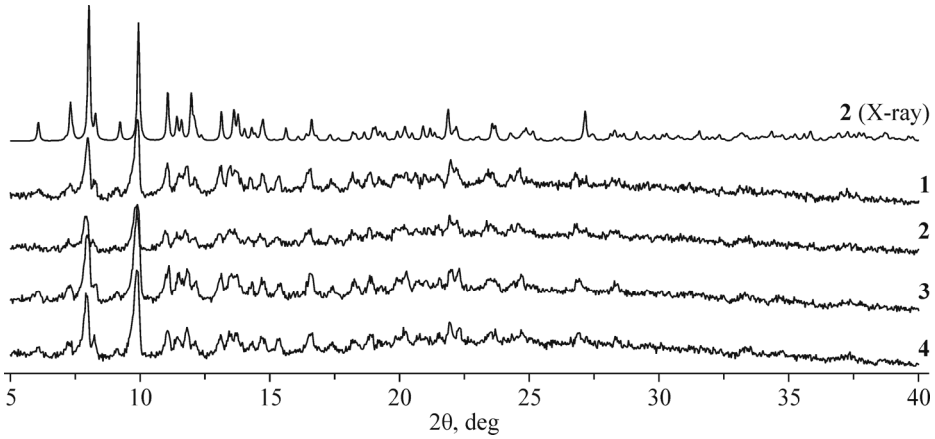

Fig. 4. Experimental XRD patterns of compounds **1**-**4** and the theoretical XRD pattern of compound **2** (X-ray crystallography).

in the ranges ~1340-1450 cm^{-1} and ~1500–1630 cm^{-1} correspond to stretching vibrations of the double bonds of **L** aromatic rings (ν(C=C) and ν(C=N)). The band at 1712 cm^{-1} corresponds to stretching vibrations of C=O bonds of solvate acetone molecules [34].

The temperature dependence of μ_{eff} for complexes **1**-**4** is depicted in Fig. 5*a*. The μ_{eff} values for compounds **1** and **2** at 300 K are 3.14 μ_B and 6.08 μ_B and gradually decrease with decreasing temperature, reaching 1.04 μ_B and 0.62 μ_B, respectively, at 2 K. This behavior of the $\mu_{эфф}(T)$ dependence is typical of Sm^{3+} and Eu^{3+} compounds for which the ground states are $^6H_{5/2}$ and $^7F_0$ respectively, but there are levels with close energies and different J [34]. An expression for the magnetic susceptibility of the Sm^{3+} ion does not well describe the experimental $\mu_{eff}(T)$ dependence for complex **1** in the low-temperature range but allows the estimation of the spin-orbit interaction parameter $\lambda \approx 210$ cm^{-1}. For compound **2** the $\mu_{eff}(T)$ dependence is described well by the expression for the magnetic susceptibility of the Eu^{3+} ion; the optimal λ value obtained from the analysis of the $\mu_{eff}(T)$ dependence is 293 cm^{-1}.

The μ_{eff} values for compounds **3** and **4** at 300 K are 16.76 μ_B and 18.30 μ_B. With decreasing temperature the μ_{eff} values for **3** and **4** decrease at first gradually and below 50 K and 100 K respectively abruptly decrease, reaching 12.27 μ_B and 12.87 μ_B at 2 K (Fig. 5*a*). A decrease in μ_{eff} at low temperatures is due to a splitting in the ligand field. In the temperature range 300-50 K the $1/\chi(T)$ dependence for complexes **3** and **4** obey the Curie–Weiss law: optimal Curie (C) and Weiss (θ)

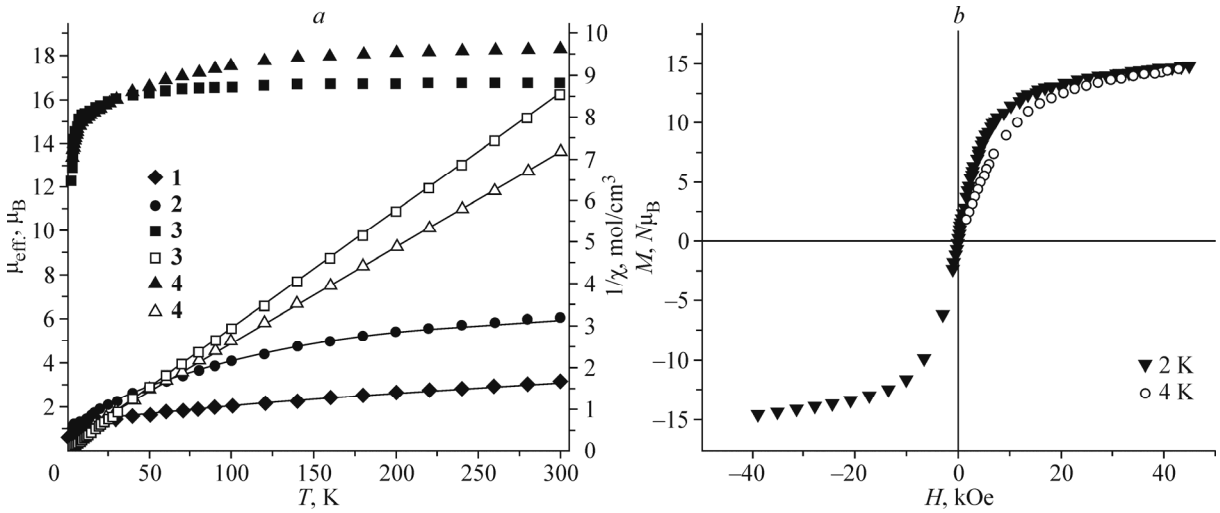

Fig. 5. Dependences $\mu_{eff}(T)$ (black) for complexes **1**, **2**, **3**, **4** and $1/\chi(T)$ (white) for complexes **3**, **4**; calculated curves are shown by solid lines (*a*); field dependences of the magnetization of complex **3** at T = 2 K (*1*) and 4 K (*2*) (*b*).

constants are 35.37 K·cm^3/mol and –2.5 K for **3**, 43.91 K·cm^3/mol and –14.1 K for **4**. For **3** and **4** the μ_{eff} values at 300 K and the Curie constant C agree well with theoretical values of 16.84 μ_B and 35.44 K·cm^3/mol for three Tb^{3+} ions (ground state $^7F_6$, g_J = 4/3), 18.44 μ_B and 42.5 K·cm^3/mol for three Dy^{3+} ions (ground state $^6H_{15/2}$, g_J = 4/3).

The dependence of the magnetization M on the external magnetic field strength H for compound **3** at a low temperature is nonlinear and comes to saturation of ~15 $N\mu_B$, which is lower than the theoretical value of 27 $N\mu_B$ for three Tb^{3+} ions (Fig. 5*b*).

Fig. 6 depicts luminescence excitation and PL spectra of **L** and complexes **1**-**4**, and also the emission spectrum of polycrystalline phen·H_2O at 300 K. In the excitation spectrum of the free **L** ligand there is a broad band with maxima at 340 nm, 356 nm, and 368 nm. The PL spectrum of the **L** ligand has vibrational components with maxima at 391 nm, 407 nm, and ~435 nm and a long structureless tail up to 600 nm (Fig. 6*a*). The introduction of the phen moiety containing a terpene residue into the molecule causes a substantial narrowing of the emission band of the **L** ligand and a 47 nm shift of the emission maximum to the short-wave range as compared to unsubstituted phen. The absolute quantum yield of **L** luminescence is 6.0%. The luminescence kinetics of the **L** ligand and complexes **1**-**4** in the solid state is intricate and is processed well in the one-, two-, or three-exponential approximation (Fig. 7)

$$I(t) = A_1 e^{-\frac{t}{\tau_1}} + A_2 e^{-\frac{t}{\tau_2}} + A_3 e^{-\frac{t}{\tau_3}}.$$

The intricate kinetics is characteristic of the luminescence of solid samples of many compounds. The fluorescence time distribution is related to a heterogeneous local environment of molecules in microcrystals. Some molecules are located near crystal lattice defects and the others are located on the crystal surface. Moreover, a high concentration of molecules in the crystals can cause the migration of excitation and emission on centers with lower-lying levels.

At the maximum of the first vibrational component (391 nm) of the **L** ligand, the kinetics is well approximated by two exponents with times τ_1 = 1.5 ns (0.05%) and τ_2 = 3.3 ns (99.95%) (the percentage of emitted quanta in each exponent is given in parentheses, which was calculated by the formula $N_i = 100 \times A_i\tau_i / \sum A_i\tau_i$).

For complex **1** in the solid state the ligand luminescence is absent and only a spectrum of characteristic orange Sm^{3+} luminescence appears (Fig. 6*b*). The PL spectrum of complex **1** contains four split bands corresponding to 4*f*–4*f* transitions in the Sm^{3+} ion at 565 nm ($^4G_{5/2} \rightarrow {}^6H_{5/2}$ transition), 601 nm ($^4G_{5/2} \rightarrow {}^6H_{7/2}$), 650 nm ($^4G_{5/2} \rightarrow {}^6H_{9/2}$), and 713 nm ($^4G_{5/2} \rightarrow {}^6H_{11/2}$). In the excitation spectrum of **1** (λ_{em} = 642 nm) a broad band with the maximum at 370 nm is observed, which corresponds to excitation of the organic chromophore ($S_0 \rightarrow S_1$) [36]. The luminescence quantum yield of **1** is 1.8%. For **1** the luminescence decay kinetics is well described by one exponent with τ = 1.1 ns (Fig. 7*b*).

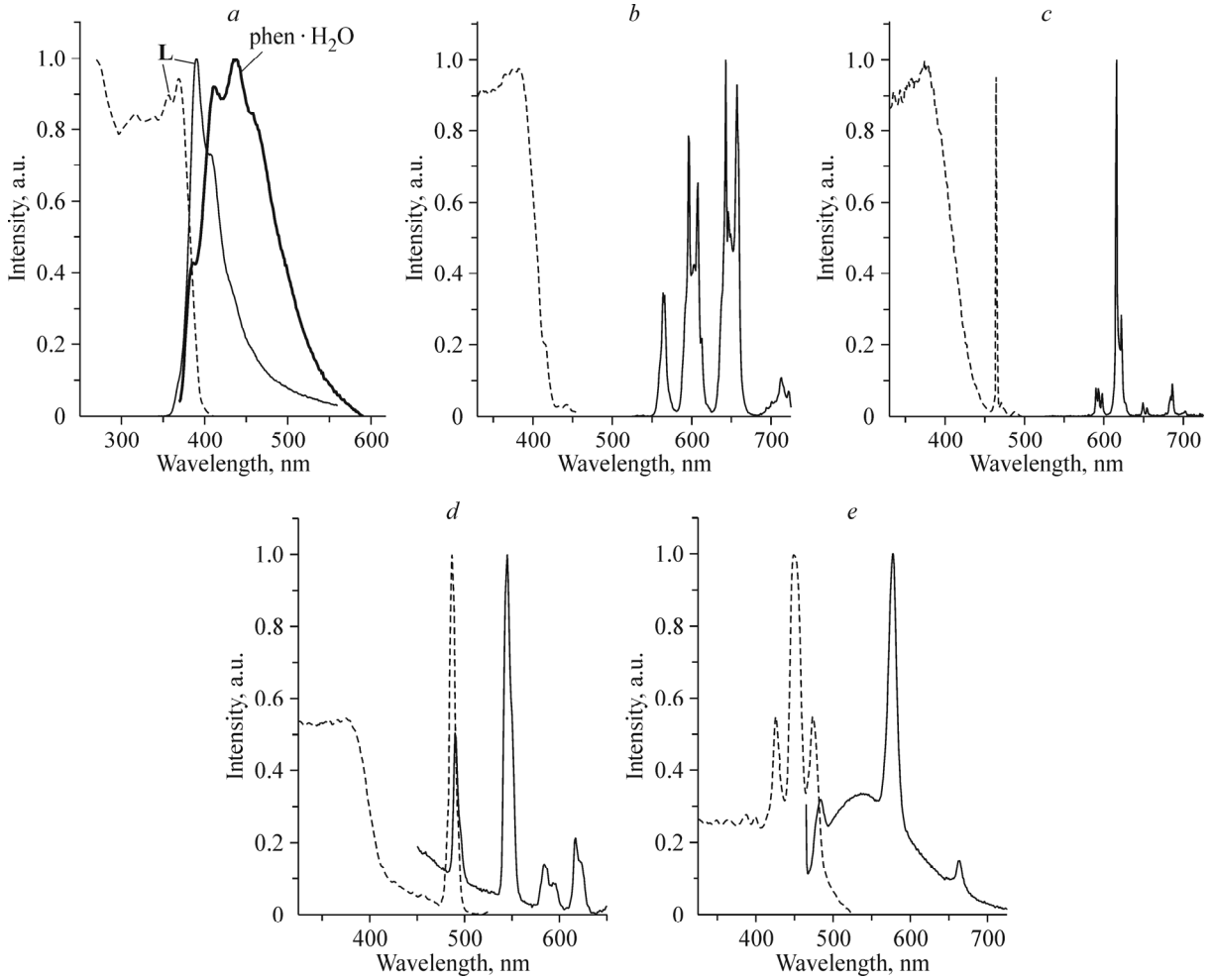

Fig. 6. Normalized luminescence excitation spectra (dotted lines) and PL spectra (solid lines) of solid phases of the compounds at 300 K: **L** and phen·H_2O (*a*); **1** (*b*); **2** (*c*); **3** (*d*); **4** (*e*). Luminescence excitation at a wavelength of 370 nm.

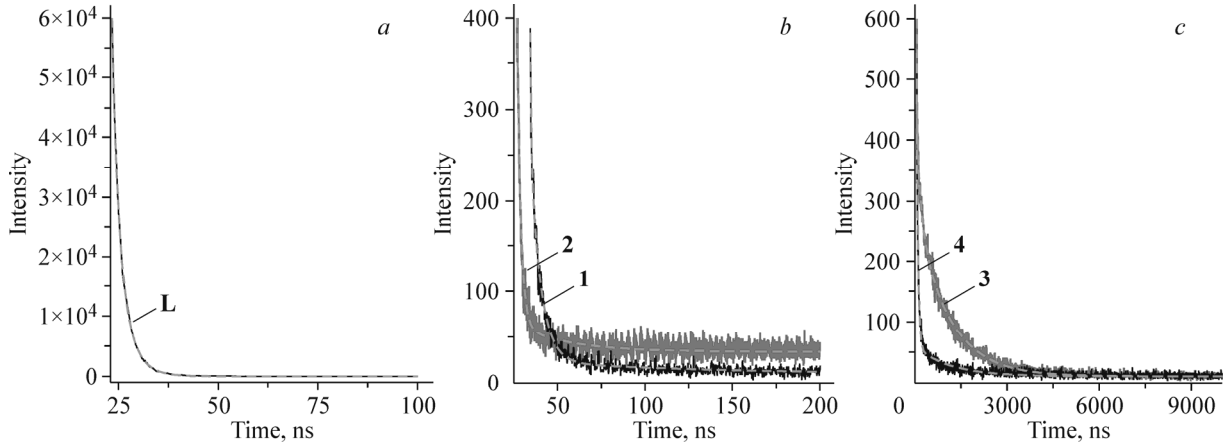

Fig. 7. Luminescence kinetics of solid phases: **L** ligand (*a*); complexes **1**, **2** (*b*); complexes **3**, **4** (*c*). Luminescence excitation at a wavelength of 350 nm. Calculated curves are shown by dashed lines.

In the red PL spectrum of complex **2** split bands are observed at 593 nm, 615 nm, 647 nm, and 686 nm in the Eu^{3+} ion, which correspond to $^5D_0 \rightarrow {}^7F_j$ (j = 1-4) transitions respectively (Fig. 6*c*). The luminescence excitation spectrum of **2** (λ_{reg} = 615 nm) exhibits a broad band with the maximum at 375 nm, which corresponds to the $S_0 \rightarrow S_1$ transition in the ligand and a narrow band at 465 nm, which corresponds to the intraconfigurational $^7F_0 \rightarrow {}^5D_2$ *f–f* transition from the Eu^{3+} ground state. The luminescence quantum yield of compound **2** is 4.7%. The luminescence kinetics at a wavelength of 615 nm is approximated by one exponent with τ = 0.6 ns (Fig. 7*b*). The luminescence lifetime is consistent with the luminescence lifetime of many Eu(III) complexes with organic ligands. However, it should be noted that Eu^{3+} complexes with longer luminescence lifetimes have also been known [25].

For **3** in the solid state, a spectrum of characteristic green Tb^{3+} luminescence is measured with maxima at 491 nm, 546 nm, 585 nm, and 622 nm (Fig. 6*d*), which correspond to $^5D_4 \rightarrow {}^7F_j$ (j = 6-3) transitions. In the luminescence excitation spectrum of **3** (λ_{em} = 545 nm) a broad band is observed with the maximum at 375 nm ($S_0 \rightarrow S_1$ transition in the ligand) and a narrow band at 487 nm ($^7F_6 \rightarrow {}^5D_4$ transition in the Tb^{3+} ion). The $S_0 \rightarrow S_1$ band has a lower intensity than the $^7F_6 \rightarrow {}^5D_4$ band, which testifies to a low-efficient sensibilization process of Tb^{3+} luminescence by the **L** ligand. The luminescence quantum yield is less than 0.5%. Luminescence at a wavelength of 545 nm has complicated kinetics with three times of exponents: τ_1 = 0.01 μs (64.1%), τ_2 = 0.1 μs (3.6%), and τ_3 = 1.1 μs (32.3%) (Fig. 7*c*).

Complex **4** in the solid state exhibits low-intensity luminescence; its bands are measured at 484 nm, 577 nm, and 663 nm, which correspond to $^4F_{9/2} \rightarrow {}^6H_{j/2}$ (j = 13, 11, 9) transitions respectively in the Dy^{3+} ion (Fig. 6*e*). In the excitation spectrum of **4** (λ_{em} = 575 nm) the $S_0 \rightarrow S_1$ band is much less intense than the intraconfigurational *f–f* bands at 426 nm ($^6H_{15/2} \rightarrow {}^4G_{11/2}$), 452 nm ($^6H_{15/2} \rightarrow {}^4I_{15/2}$), 474 nm ($^6H_{15/2} \rightarrow {}^4F_{9/2}$), which indicates the inefficient sensibilization of Dy^{3+} luminescence in this compound. We failed to determine the quantum yield of the compound. The luminescence decay kinetics of **4** is well described by two exponents with τ_1 = 1.2 μs (46.1%) and τ_2 = 0.47 μs (53.9%) (Fig. 7*c*).

Thus, the luminescence quantum yield decreases in the series of compounds **2** > **1** > **3** ≈ **4**. The absence of bright emission of compounds **3** and **4** is likely to be due to bad correspondence between the lowest ligand-centered triplet state T_1 and the ground emission states of Tb^{3+} ($^5D_4$) and Dy^{3+} ($^6H_{15/2}$) ions, which lead to the inefficient sensibilization of luminescence of these ions by the **L** ligand.

CONCLUSIONS

As a result of the performed work, a new group of complexes of trivalent lanthanides containing a chiral dextrorotatory ligand based on 1,1-phen and (+)–3-carene was obtained and studied. The ionic complexes crystallize in the non-centrosymmetric space group *P*1; CN of Ln atoms is 10. The $\mu_{eff}(T)$ dependence of compounds in the temperature range 2-300 K is characteristic of Ln^{3+} complexes. The dependence of the magnetization of the Dy^{3+} complex on the external magnetic field strength is nonlinear. In the coordination compounds there is the energy transfer process from the triplet level of the excited ligand to Ln *f*-levels, which causes the appearance of characteristic luminescence of lanthanides. In all cases, the compounds in the solid state had the complicated luminescence kinetics described by one, two, or three exponents.

ACKNOWLEDGMENTS

The authors are thankful to A.P. Zubareva and V.V. Ankudovich for the elemental analysis data, P.E. Plyusnin for the thermogravimetry data, N.I. Alferova for the IR spectra, and N.P. Korotkevich for the powder XRD data.

FUNDING

The study was supported by RFBR within scientific project No. 18-33-00239.

CONFLICT OF INTERESTS

The authors declare that they have no conflict of interests.

REFERENCES

1. G. F. De Sa, O. L. Malta, C. de Mello Donega, A. M. Simas, R. L. Longo, P. A. Santa-Cruz, and E. F. da Silva Jr. *Coord. Chem. Rev.*, **2000**, *196*, 165.
2. J.-C. G. Bünzli. *Acc. Chem. Res.*, **2006**, *39*, 53.
3. J.-C. G. Bünzli and S. V. Eliseeva. *Chem. Science*, **2013**, *4*, 1939.
4. M. D. Allendorf, C. A. Bauer, R. K. Bhakta, and R. J. T. Houk. *Chem. Soc. Rev.*, **2009**, *38*, 1330.
5. L. Armelao, S. Quici, F. Barigelletti, G. Accorsi, G. Bottaro, M. Cavazzini, and E. Tondello. *Coord. Chem. Rev.*, **2010**, *254*, 487.
6. M. A. Katkova, A. G. Vitukhnovsky, and M. N. Bochkarev. *Russ. Chem. Rev.*, **2005**, *74*, 1089.
7. M. A. Katkova and M. N. Bochkarev. *Dalton Trans.*, **2010**, *39*, 6599.
8. M. N. Bochkarev, A. G. Vitukhnovsky, and M. A. Katkova. Organic Light Emitting Diodes (OLED). DEKOM: Nizhny Novgorod, **2011**.
9. S. V. Larionov and Yu. A. Bryleva. *Russ. J. Coord. Chem.*, **2016**, *42*, 293.
10. G. Accorsi, A. Listorti, K. Yoosaf, and N. Armaroli. *Chem. Soc. Rev.*, **2009**, *38*, 1690.
11. D. L. Kepert, L. I. Semenova, A. N. Sobolev, and A. H. White. *Aust. J. Chem.*, **1996**, *49*, 1005.
12. D.-Y. Wei, J.-L. Lin, and Y.-Q. Zheng. *J. Coord. Chem.*, **2002**, *55*, 1259.
13. Y.-Q. Zheng, L.-X. Zhou, J.-L. Lin, and S.-W. Zhang. *Z. Anorg. Allg. Chem.*, **2001**, *627*, 1643.
14. A. G. Mirochnik, B. V. Bukvetskii, P. A. Zhikhareva, and V. E. Karasev. *Russ. J. Coord. Chem.*, **2001**, *27*, 443.
15. G. G. Sadikov, A. S. Antsyshkina, I. A. Kuznetsova, and M. N. Rodnikova. *Crystallogr. Rep.*, **2006**, *51*, 47.
16. Z. Pan, G. Jia, C.-K. Duan, W.-Y. Wong, W.-T. Wong, and P. Tanner. *Eur. J. Inorg. Chem.*, **2011**, *5*, 637.
17. G. G. Sadikov, A. S. Antsyshkina, M. N. Rodnikova, and I. A. Solonina. *Crystallogr. Rep.*, **2009**, *54*, 48.
18. I. V. Ananyev, Yu. V. Nelyubina, L. N. Puntus, K. A. Lyssenko, and I. L. Eremenko, *Russ. Chem. Bull.*, **2016**, *65*, 1178.
19. P. A. Tanner. *Coord. Chem. Rev.*, **2010**, *254*, 3026.
20. L. N. Puntus and V. F. Zolin. *Russ. J. Coord. Chem.*, **2003**, *29*, 574.
21. G. Muller. *Dalton Trans.*, **2009**, *44*, 9692.
22. J. Crassous. *Chem. Soc. Rev.*, **2009**, *38*, 830.
23. G. Muller, J.-C. G. Bunzli, J. P. Riehl, D. Suhr, A. von Zelewsky, and H. Mürner. *Chem. Commun.*, **2002**, *14*, 1522.
24. J. Liu, X.-P. Zhang, T. Wu, B. B. Ma, T. W. Wang, C. H. Li, Y. Z. Li, and X. Z. You. *Inorg. Chem.*, **2012**, *51*, 8649.
25. S. V. Larionov, Yu. A. Bryleva, L. A. Glinskaya, V. F. Plyusnin, A. S. Kupryakov, A. M. Agafontsev, A. V. Tkachev, A. S. Bogomyakov, D. A. Piryazev, and I. V. Korolkov. *Dalton Trans.*, **2017**, *46*, 11440.
26. J. Lewis and T. D. O′Donoghue. *Dalton Trans.*, **1980**, *5*, 736.
27. A. V. Tkachev and A. V. Rukavishnikov. *Mendeleev Comm.*, **1992**, *4*, 161.
28. S. A. Popov, A. Yu. Denisov, Yu. V. Gatilov, I. Yu. Bagryanskaya, and A. V. Tkachev. *Tetrahedron: Asymmetry*, **1994**, *3*, 479.
29. G. M. Sheldrick. *Acta Crystallogr.*, **2015**, *71*, 3.
30. F. W. Lewis, L. M. Harwood, M. J. Hudson, M. G. B. Drew, J. F. Desreux, G. Vidick, N. Bouslimani, G. Modolo, A. Wilden, M. Sypula, T.-H. Vu, and J.-P. Simonin. *J. Am. Chem. Soc.*, **2011**, *133*, 13093.
31. M. Steppert, I. Císařová, T. Fanghänel, A. Geist, P. Lindqvist-Reis, P. Panak, P. Štěpnička, S. Trumm, and C. Walther. *Inorg. Chem.*, **2012**, *51*, 591.

32. V. Tsaryuk, V. Zolin, L. Puntus, V. Savchenko, J. Legendziewicz, J. Sokolnicki, and R. Szostak. *J. Alloys Compd*., **2000**, *300–301*, 184.
33. I. R. Ferraro. *J. Mol. Spectr*., **1960**, *4*, 99.
34. K. Nakamoto. Infrared and Raman Spectra of Inorganic and Coordination Compounds Pt. A. USA, Wiley: Hoboken, **2009**.
35. M. Andruh, E. Bakalbassis, O. Kahn, J. C. Trombe, and P. Porchers. *Inorg. Chem*., **1993**, *32*, 1616.
36. M. D. Regulacio, M. H. Publico, J. A. Vasquez, P. N. Myers, S. Gentry, M. Prushan, S.-W. Tam-Chang, and S. L. Stoll. *Inorg. Chem*., **2008**, *47*, 1512.